Local structure, optical and magnetic studies of Ni nanostructures embedded in a SiO_2 matrix by ion implantation

2008 J. Phys.: Condens. Matter 20 285211

(http://iopscience.iop.org/0953-8984/20/28/285211)

J. Phys.: Condens. Matter **20** (2008) 285211 (8pp) doi:10.1088/0953-8984/20/28/285211

Local structure, optical and magnetic studies of Ni nanostructures embedded in a SiO_2 matrix by ion implantation

S K Sharma[1,5], P Kumar[2], Ravi Kumar[2], M Knobel[1], P Thakur[3], K H Chae[3], W K Choi[3], R Kumar[4] and D Kanjilal[2]

[1] Instituto de Fisica Gleb Wataghin, Universidade Estadual de Campinas (UNICAMP) Campinas, 13.083-970, SP, Brazil
[2] Inter-University Accelerator Centre (IUAC), New Delhi 110 067, India
[3] Materials Science and Technology Research Division, KIST, Seoul 136-791, Korea
[4] Department of Physics, Chaudhary Charan Singh University, Meerut 250 004, UP, India

E-mail: surender76@gmail.com and sharma@ifi.unicamp.br

Received 13 December 2007, in final form 26 April 2008
Published 17 June 2008
Online at stacks.iop.org/JPhysCM/20/285211

Abstract

This work reports the formation of Ni nanostructures, their growth and saturation to form oxides by using ion implantation and thermal treatment in air at 600 °C. A quartz (SiO_2) matrix was implanted with 100 keV Ni^+ ions to doses in the range 5×10^{15}–2×10^{17} ions cm^{-2}. The formation of Ni nanoclusters was observed by high resolution x-ray diffraction (HRXRD), UV–visible optical spectroscopy, dc magnetization, AFM/MFM and x-ray absorption spectroscopy (XAS). The cluster size distribution is narrow, with an average size of $\sim 25 \pm 0.5$ nm for the sample implanted at a dose of 1×10^{16} ions cm^{-2}, but increases with implantation dose. Optical absorption spectra also show a clear signature of a surface plasmon resonance (SPR) peak at around 388 nm in accordance with the theoretical Mie's spectra. Temperature dependent zero-field-cooled and field-cooled magnetization measurements clearly indicate a superparamagnetic behavior, which is properly analyzed considering the size distribution of the magnetic nanostructures. The results show that the magnetic properties of the nanoparticles can be controlled by the implantation dose. A detailed investigation of the local structure using Ni K-edge NEXAFS/EXAFS suggests that the size of the Ni nanostructures is altered by implantation dose, reaching saturation in the form of oxides/silicates of Ni at a dose of 2×10^{17} ions cm^{-2}.

(Some figures in this article are in colour only in the electronic version)

1. Introduction

Nanostructured materials play an important role in future technology as they exhibit different and often unique physical properties relative to their macroscopic counterparts. Metal nanoparticles in insulators with low dielectric constants have the advantage of exhibiting single electron effects at high temperatures, since the total capacitance of the dots decreases in these materials [1]. Metallic nanoparticles embedded in insulators are being extensively studied because of their interesting electrical, magnetic, magneto-optic, catalytic and optical properties including surface plasmon resonance (SPR) and third-order nonlinear optical susceptibility [2–5]. The presence of nanostructures can give rise to composites with very large values of third-order susceptibility $\chi^{(3)}$ related to high nonlinear refractive index term n_2, defined by $n = n_0 + n_2 I$, where n_0 is the base index and I the light intensity [6]. Moreover, magnetic nanoparticles are expected to exhibit interesting effects [7], such as superparamagnetic behavior [8], tunneling magnetoresistance [9] and giant Hall Effect [10]. Such composites have drawn much attention owing to their applicability for fast switching devices, single electron transistors, gas sensors and nanoelectronics in one-

[5] Author to whom any correspondence should be addressed.

dimensional molecular wires [11–13]. The possibility of using these nanocomposites not only on fundamental studies, but also for creating new devices, is stimulating a rather strong research effort to control several variables, such as the nanocluster size distribution, their shape, as well as the inter-particle distances. Several techniques are used for preparation of such type of nanocomposites such as sputtering from a composite target, sequential sputtering, laser ablation, plasma jet and ion implantation, for example [14–16]. The ion implantation technique [16, 17] is a well-established procedure to obtain nanocomposites of a wide range of metals and insulators. In general, ion implantation is a non-equilibrium process, which leads to the formation of novel phases, metastable structures and induces strain in the host matrix and precipitates the implanted ions as nanoclusters. Much research is concentrated on the optical properties of silica glasses and metallic nanoclusters synthesized by ion implantation including Ag, Au, Ga and other transition metal elements [18–20]. In the case of Ni and Co implanted silica [16, 21, 22], metallic nanostructures are formed in the host matrix, whereas the sequential implantation of Ni and Co gives rise to Ni–Co alloy based nanoparticles. Amekura *et al* [23] have investigated the formation of NiO nanoparticles in SiO_2 from the thermal oxidation of Ni/SiO_2 nanocomposites by using this technique. Ding *et al* [24] had also shown similar oxidation effects in the case of a Fe implanted SiO_2 matrix. Recently, Lobotka *et al* [3] have shown the single electron transport phenomenon in the case of isolated Fe nanoparticles in a SiO_2 matrix. Indeed, the technique allows one to obtain well controlled nanostructures by choosing suitable ion implantation conditions and successive thermal treatment. Furthermore, the technique would be compatible with large scale integration of the device fabrication process. However, understanding the structural evolution during the preparation of nanocomposite materials can be of great help in understanding how to control the characteristics of the final products.

In this paper, we present the synthesization of Ni nanoparticles embedded in a SiO_2 matrix using ion implantation and their characterization using high resolution x-ray diffraction (HRXRD), atomic force microscopy (AFM), magnetic force microscopy (MFM), dc magnetization and UV–visible absorption spectroscopy. The local structure and its evolution were studied by means of x-ray absorption spectroscopy (XAS) techniques. XAS is a useful tool to examine nanosized particles of Ni implanted into the quartz matrix and to gain information about the presence and nature of the interactions among metal atoms and quartz networks. Also, it allows the study of the influence of ion implantation conditions on the structural evolution of metal (or metal oxide) nanoparticles in Ni-SiO_2 (quartz) nanocomposites. Quantitative structural information about the metal environment in complex materials can be obtained from extended x-ray absorption fine structure (EXAFS) spectra, whereas near edge x-ray absorption fine structure (NEXAFS) can provide electronic and structural information around each atom. In the present study, we have examined the valance state and coordination state of implanted nickel ions in a quartz matrix using x-ray absorption fine structure (XAFS) spectroscopy, both by EXAFS and NEXAFS techniques.

2. Experimental details

The implantation of 100 keV Ni^+ ions was performed in a SiO_2 matrix at room temperature for doses ranging from 5×10^{15} to 2×10^{17} ions cm^{-2} in a vacuum chamber of 1.3×10^{-6} Torr using an electron cyclotron resonance (ECR) ion source (placed on a high voltage platform) based low energy ion beam facility (LEIBF) [25] at IUAC, New Delhi. An ion current density of 2.8 μA cm^{-2} was maintained during the implantation of samples to avoid local heating. At this energy, the projected range and straggling are 78.2 nm and 22 nm, respectively, according to Monte Carlo simulations performed with the SRIM code 2006. After implantation, the samples were post-annealed at 600 °C in air for 4 h.

The formation of nanostructures was observed initially by HRXRD, with $\lambda = 1.5425$ Å at the bending magnet 10C1 XRD II beamline of the Pohang Accelerator Laboratory (PAL), operating at 2.5 GeV with a maximum storage current of 200 mA, and the surface morphology and magnetic domain formation by AFM/MFM using Digital NanoScope-III. The optical absorption measurements were performed using an Hitachi UV–visible absorption spectrometer and the data were properly analyzed according to Mie's theory for the absorption of light by small metallic spheres [26, 27].

The magnetic properties of nanostructures were also characterized by means of zero-field-cooling (ZFC) and field-cooling (FC) magnetization measurements in a Quantum Design MPMS SQUID Magnetometer, in the temperature range $5\ K < T < 300\ K$ with a magnetic field of 100 Oe parallel to the surface of the sample. The diamagnetic contribution from the SiO_2 was subtracted from the measured data by performing the magnetization of the unimplanted SiO_2 sample with similar dimensions at room temperature.

The O K- and Ni $L_{3,2}$-edges NEXAFS spectra of all the samples along with NiO and SiO_2 were measured at the beamline 7B1 XAS KIST of the PAL in total electron yield (TEY) mode and the fluorescence yield (FY) mode at room temperature in a vacuum better than 1.5×10^{-8} Torr. The spectra in the two modes turned out to be nearly identical indicating that the systems are so stable that the surface contamination effects are negligible even in the TEY mode. All the spectra were normalized to the incident photon flux and the energy resolution was better than 0.2 eV. For Ni K-edge experiments, the 5A HFMS (Wiggler) beamline of the PAL was utilized. The beam was monochromatized by a cryogenic double-crystal Si(111) monochromator detuned from 20 to 30%, depending upon the Ni ion concentration in the samples, to suppress higher-order harmonic content from the beam. All the scans were made at room temperature in fluorescence detection mode using a Bent Crystal Laue Analyzer (BCLA) detector system. The advantage of using BCLA is that it allows the isolation of unwanted energies (noise) from fluorescence signals, thereby significantly improving the data quality. The resolution of the monochromator is about 1 eV in the studied energy range. Spectra for reference samples namely Ni metal foil and NiO nanopowder were also recorded in transmission mode. The data sets were aligned and backgrounds were removed using

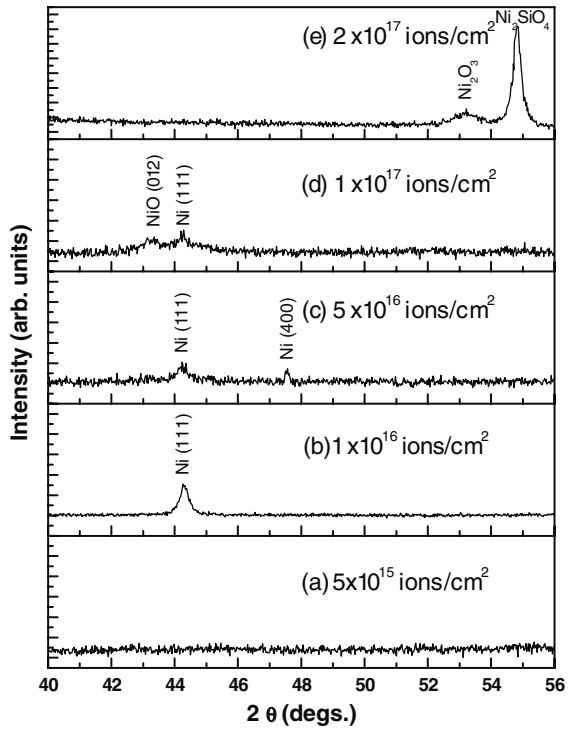

Figure 1. High resolution x-ray diffraction (HRXRD) corresponding to Ni implanted SiO_2 at doses (a) 5×10^{15}, (b) 1×10^{16}, (c) 5×10^{16}, (d) 1×10^{17}, and (e) 2×10^{17} ions cm^{-2}.

the standard ATHENA program [28], which is based on the AUTOBK to remove the background. The input parameter to ATHENA that determines the maximum frequency of the background R_{bkg} was set to 1.1 Å. The data range used for Fourier transforming the k space data was 2.3–9.8 Å^{-1}. A Hanning window function was used with a dk of 1.0.

3. Results and discussion

Figure 1 shows the HRXRD patterns recorded for the various doses of 100 keV Ni^+ implanted (or annealed) samples in the range 5×10^{15}–2×10^{17} ions cm^{-2}. From the patterns, it is clearly seen that no Ni peak appears for the sample implanted at a dose of 5×10^{15} ions cm^{-2}. However, with the increase in the implantation dose to a value 1×10^{16} ions cm^{-2}, the structure starts growing and a broad peak is observed at $2\theta = 44.30°$. Diffraction line profile analysis performed on this peak, assuming an fcc phase of Ni(111) gives a lattice parameter, $a = 0.3582 \pm 0.001$ nm, which is comparable with the bulk Ni lattice parameter (Ni, JCPDS card no. 87-0712). The corresponding average size of the nanoclusters, calculated using the Scherrer formula was $\sim 25 \pm 0.5$ nm. With a further increase in the implantation dose to 5×10^{16} ions cm^{-2}, the XRD pattern exhibits a new diffraction peak at $2\theta = 47.55°$ along with Ni(111), which is near to the reflections of bulk Ni(400) (JCPDS card no. 01-1266). However, at a dose 1×10^{17} ions cm^{-2}, in addition to Ni(111) phase, the pattern consists of (012) NiO phase (JCPDS card no. 47-10479) located at $2\theta = 43.24°$. Finally, at the highest implantation dose 2×10^{17} ions cm^{-2}, the only dominating phase is either nickel oxide (Ni_2O_3) or nickel silicate (Ni_2SiO_4) (JCPDS card no. 14-0481 or no. 83-1740).

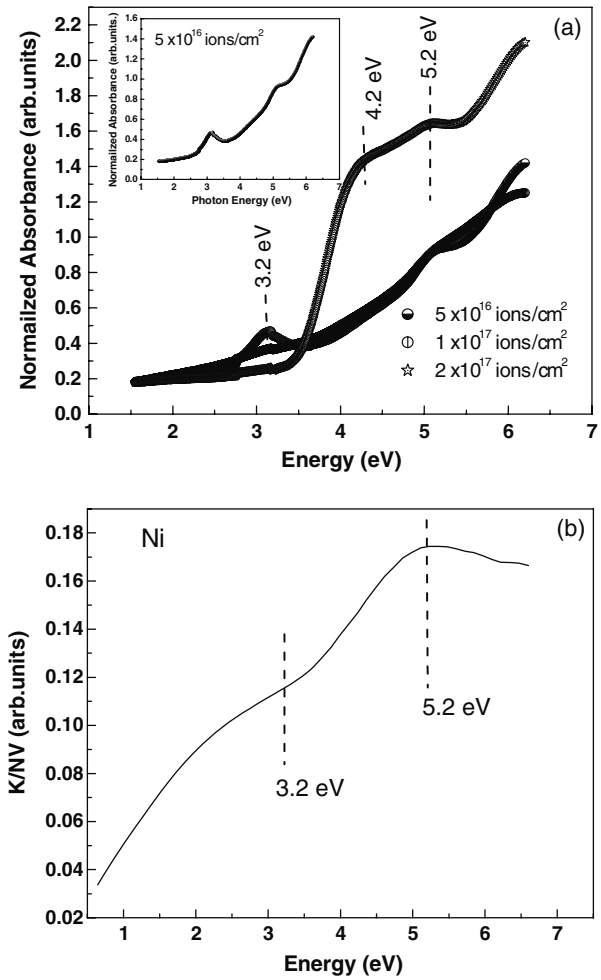

Figure 2. (a) Normalized optical absorption spectra of the Ni implanted SiO_2 at three different doses 5×10^{16}, 1×10^{17}, and 2×10^{17} ions cm^{-2}. (b) Calculated optical absorption spectrum for Ni using Mie's theory.

To further understand the metallic behavior of these Ni nanostructures, we have measured the optical absorption spectra of these samples as shown in figure 2(a). In the case of the sample implanted at a dose of 5×10^{15} ions cm^{-2}, no signature of Ni nanoparticle formation was observed (not shown here), whereas for a dose of 5×10^{16} ions cm^{-2}, the presence of a SPR [27] absorption peak around 3.2 eV (388 nm) in the spectra confirmed the formation of metallic Ni nanoparticles. However, for a further increase in the implantation dose to 2×10^{17} ions cm^{-2}, the SPR peak disappears completely. This is further supported by the formation of oxides and silicates of Ni at higher implantation doses in agreement with HRXRD results. In addition, we have also observed a broad absorption band centered at around 5.2 eV for all the implanted samples and one at 4.2 eV in the case of sample implanted at the highest dose (2×10^{17} ions cm^{-2}). To explain these bands, we have compared the spectra to the theoretical Mie's spectrum [26, 27] of small, randomly distributed spherical particles of Ni (see figure 2(b)).

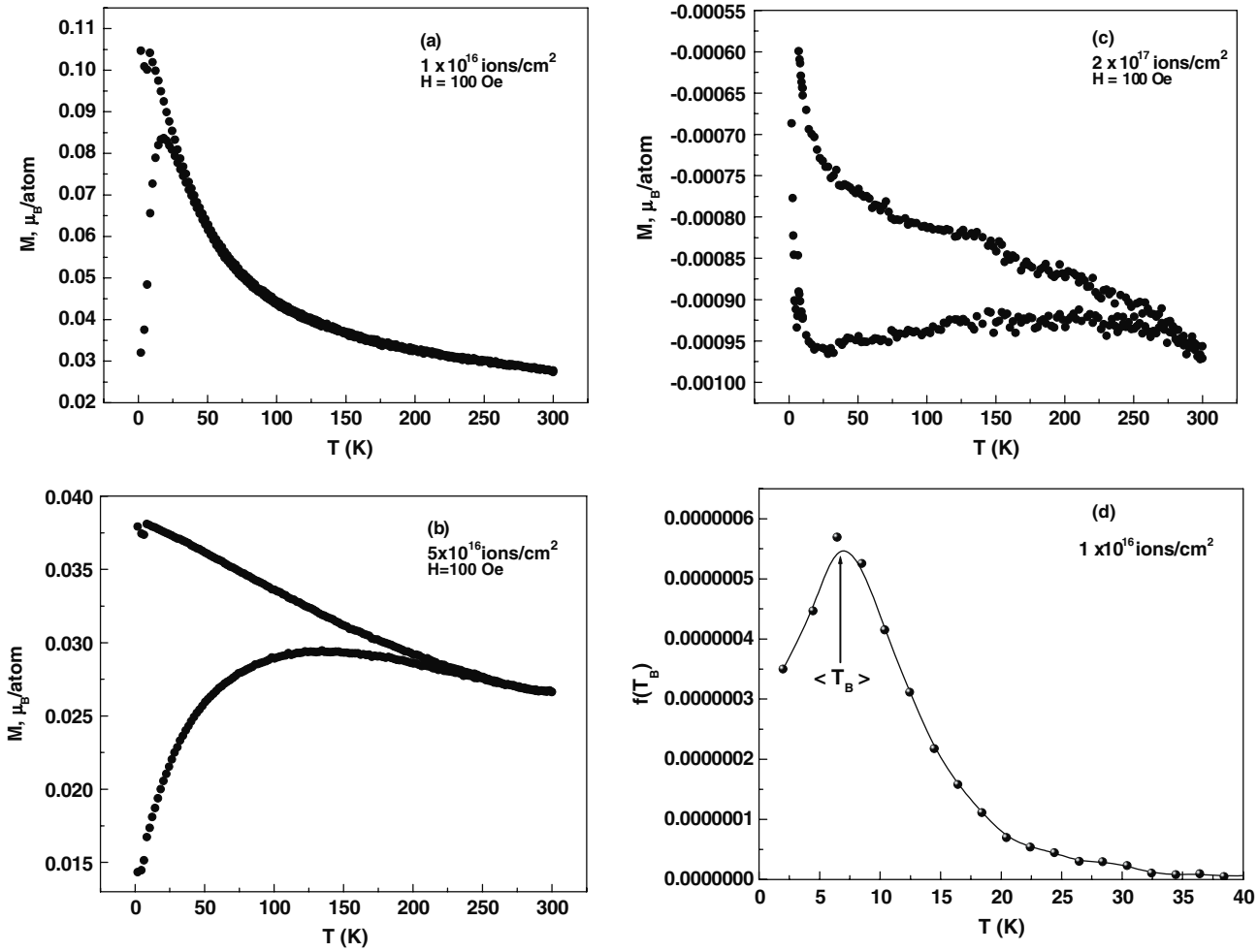

Figure 3. Magnetization versus temperature curves in zero-field-cooled (ZFC) and field-cooled (FC) modes for Ni implanted samples with different doses (a) 1×10^{16}, (b) 5×10^{16}, (c) 2×10^{17} ions cm^{-2}, and (d) the mean blocking temperature $\langle T_B \rangle$ calculated from the distribution of blocking temperatures.

According to Mie's theory, the extinction coefficient K for small particles is approximately calculated by means of the relationship [29],

$$K = (18\pi NVn^{3/2}/\lambda)(\varepsilon_2/[(\varepsilon_1 + 2n^2)^2 + \varepsilon_2^2]) \cdots \quad (1)$$

where N is the concentration of particles, V is the volume of the particle, n is the refractive index of the material medium, λ is the wavelength of the incident photon, and ε_1 and ε_2 are the real and imaginary parts of the complex dielectric constants of the particles, respectively. The spectrum was calculated by taking the refractive index of silica, the value given by Malitson [30] and the dielectric constants of Ni, those given by Johnson and Christy [31]. Creighton and Eadon [32] reported the calculated optical spectrum of Ni nanoparticles and showed a SPR absorption peak between 300 and 400 nm (4.1–3.1 eV). Also, they showed that Ni implanted silica glass exhibits absorption at 354 nm (3.4 eV) [21].

Based on these calculations, absorption bands were located at 3.2 and 5.1 eV (figure 2(b)). The former is equal to the energy 3.2 eV of the SPR; whereas latter is close to the interband transition, $L_2 \rightarrow L^1$ of Ni as reported by Ehrenreich *et al* [33] and Shiga [34]. We therefore attribute the absorption band at 3.2 eV to the SPR of Ni and that at 5.2 eV to the interband transition of Ni. Fujimori *et al* [35] also reported that optical bands of NiO/Ni_2SiO_4 at about 4 eV and 6–7 eV are assigned to interatomic 3d–3d charge transfer and O 2p–Ni 3d charge transfer, respectively. Therefore, we can infer that Ni as well as their oxides contributed to the absorption bands at energies greater than 3.2 eV, as observed for the samples implanted with doses higher than 5×10^{16} ions cm^{-2}.

To further confirm our results, we have performed magnetization versus temperature curves for these samples in zero-field-cooled (ZFC) and field-cooled (FC) modes. Figures 3(a)–(c) show the ZFC and FC magnetization as a function of temperature for various doses of Ni implantation 1×10^{16}, 5×10^{16} and 2×10^{17} ions cm^{-2}, respectively. In the ZFC mode, the sample was cooled in zero field from 300 to 5 K and after stabilization of the temperature, a measuring field of 100 Oe was applied. The data were then recorded while warming the sample. In the FC mode, the sample was cooled down from 300 to 5 K in the presence of a field of 100 Oe and then measurements were carried out while warming in the same field. In the ZFC curve, a characteristic superparamagnetic (SPM) peak confirms the

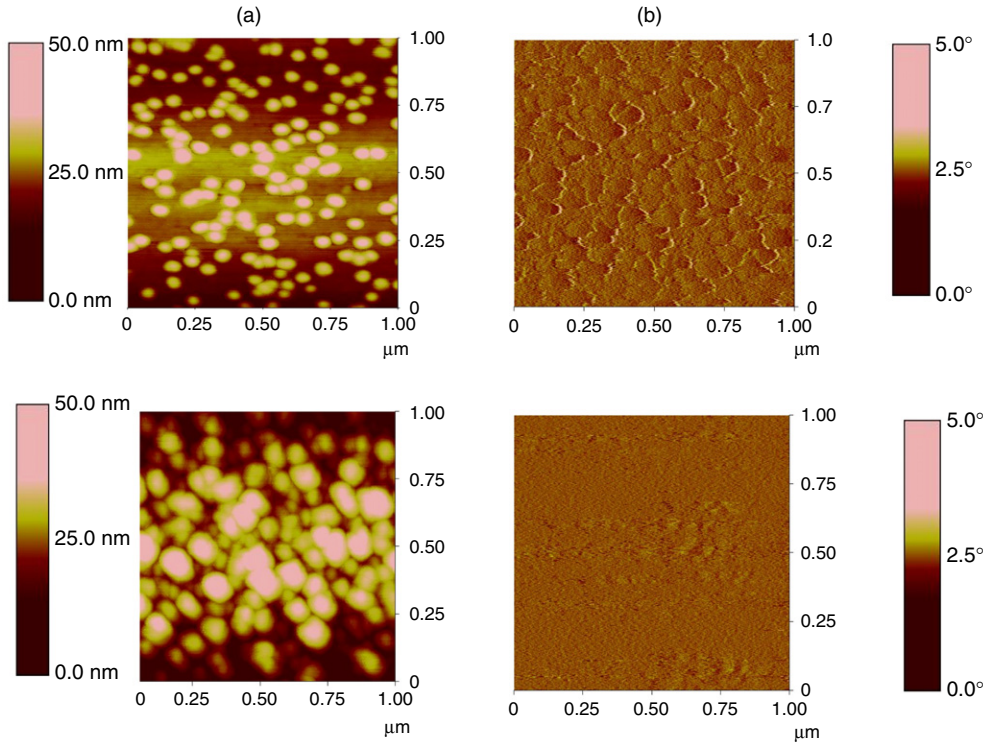

Figure 4. AFM and MFM images for (a) 1×10^{16} (top), and (b) 2×10^{17} (bottom) ions cm^{-2}.

nanoscale nature of Ni clusters. Also, the separation of ZFC and FC curves at a certain irreversibility T_{IRR} temperature is one of the characteristic features of superparamagnetism (SPM). The maximum observed on the ZFC curve T_{MEAN} (related to the mean blocking temperature T_B) is slightly lower than T_{IRR}. Such behavior indicates a particle size distribution, whereas a fraction of the largest particles already freeze at T_{IRR}, the majority fraction of the nanoparticles is being blocked at around T_{MEAN}. It is clearly evident from figure 3(a) that there is a sharp maximum in the ZFC magnetization curve at about 18 K for the 1×10^{16} ions cm^{-2} implanted sample, which indicates the mean blocking temperature of the Ni nanoclusters embedded deep inside the SiO_2 matrix. Furthermore, the relative sharpness of the ZFC peak and the fact that T_{IRR} and T_{MEAN} are quite close to each other ($T_{IRR} \sim 39$ K) can be taken as an indication of a narrow size distribution in the present case. It is worth noting that the distribution of blocking temperatures ($f(T_B)$) can be calculated as the temperature derivative of the difference between the M_{ZFC} and M_{FC} magnetizations ($d[M_{FC} - M_{ZFC}])/dT$, allowing one to correctly estimate the average blocking temperature $\langle T_B \rangle$ [36, 37]. The mean blocking temperature $\langle T_B \rangle$ calculated from the distribution of blocking temperatures was found to be ~6.4 K (see figure 3(d)). From the mean blocking temperature $\langle T_B \rangle$, we have calculated the average particle size using the Néel relaxation model for the isolated particles, i.e., $D = [(6k_B \langle T_B \rangle \ln(t_m f_0)/\pi K_{eff})]^{1/3}$, where $\langle T_B \rangle$ is the blocking temperature, K_{eff} is the anisotropic energy of Ni, t_m the measurement time, f_0 is the frequency factor and D is the size of Ni nanocluster. Considering the value 5.7×10^3 J m^{-3}, 100 s, and 10^9 s^{-1} for K_{eff} for Ni, t_m, and f_0, respectively, a value of 24.6 nm is obtained for the Ni nanocluster, which is in excellent agreement with x-ray diffraction findings. With a further increase in dose value to 5×10^{16} ions cm^{-2}, the ZFC magnetization curve became broader and centered at ~134 K (see figure 3(b)). The increase in blocking temperature clearly indicates that there is an increase in the mean particle size of the nanoclusters. The broadening in ZFC curve may be due to various reasons such as (i) broad particle size distribution, (ii) magnetic dipole–dipole interaction and (iii) some oxide formation. However, reason (iii) can be ruled out as there is no formation of Ni oxide at a dose of 5×10^{16} ions cm^{-2} in agreement with the XRD results. Indeed, as the size will grow, the distance between the nanoclusters will decrease, which will give rise to the enhancement in the component of dipole–dipole interactions. One can clearly see that the magnitude of the magnetization also did not vary linearly with the increase of Ni ions in the system, which is less than the calculated value and may be due to the dipole–dipole interaction or some oxide formation (only at dose greater than 5×10^{16} ions cm^{-2}). Figure 3(c) shows the magnetization as a function of temperature for the 2×10^{17} ions cm^{-2} implanted sample. It is found that the magnetization values are very low and almost match with the diamagnetic background of the SiO_2 substrate, which clearly indicates the formation of nickel oxide (anti-ferromagnetically ordered).

To further validate these results, we have measured the surface morphology and magnetic contrast using AFM/MFM measurements. Figures 4(a) and (b) show the AFM and MFM images taken at room temperature for 1×10^{16} and 2×10^{17} ions cm^{-2} implanted samples respectively. It is clearly seen in the AFM image (figure 4(a)) that some structures appear at the surface of similar diameter of 60 nm and

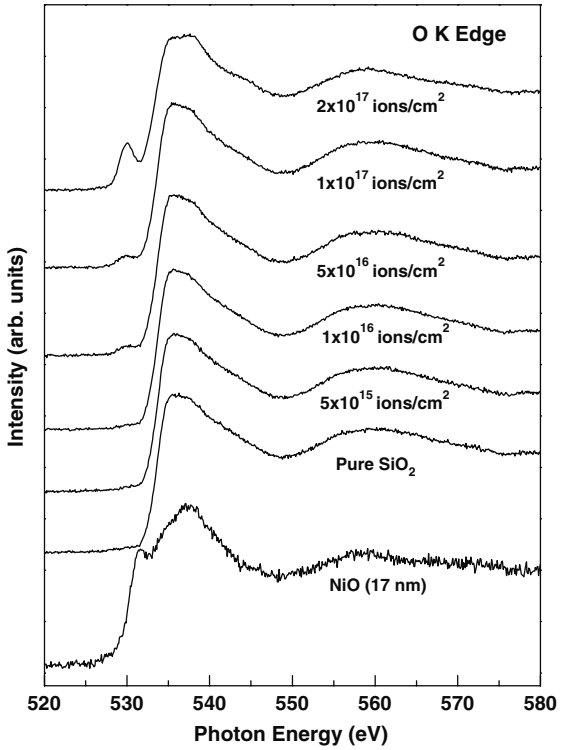

Figure 5. Normalized spectra of the O K-edge near x-ray absorption fine structure (NEXAFS) spectra of Ni implanted samples at different doses along with SiO_2 and NiO nanoparticles.

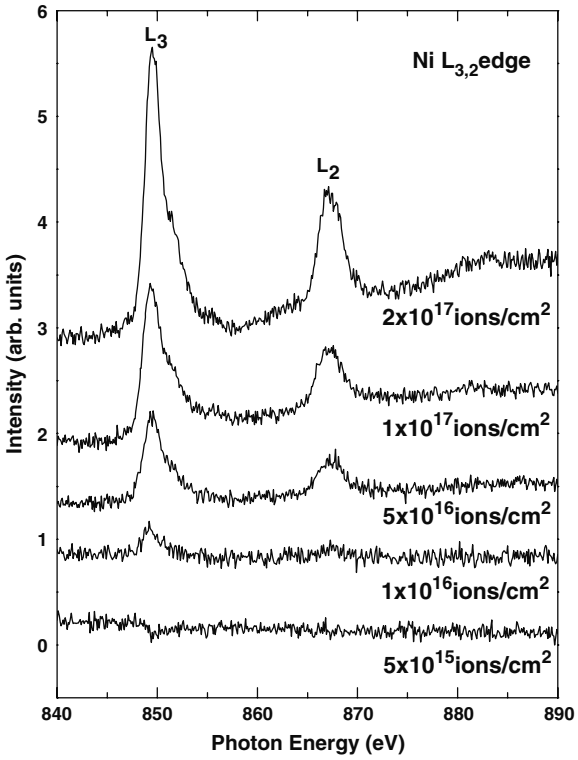

Figure 6. Normalized spectra of Ni $L_{3,2}$-edge near x-ray absorption fine structure (NEXAFS) spectra of Ni implanted samples at different doses.

height 10 nm. The MFM image taken at the lift height of 60 nm shows the clear contrast around these structures, which indicates the structure of magnetic domains. The magnetic domains are oriented in one direction along the plane of the surface. These results strengthen our hypothesis that the growth of the nanostructures is uniform with a rather narrow size distribution. On the other hand, the AFM and MFM images for the sample with an implantation dose of 2×10^{17} ions cm^{-2} indicates that the surface morphology does not show any regular structure and the magnetic contrast is also not visible, this being a signature of oxide formation of Ni particles after annealing. It is worth mentioning that before annealing no structure was formed for any implantation dose.

In order to understand the electronic and local structure of Ni nanostructures, we have performed the NEXAFS experiments at O K- and Ni $L_{3,2}$-edges for all the implanted samples along with SiO_2 and NiO nanoparticles. Figure 5 shows the normalized O K-edge NEXAFS spectra along with SiO_2 and NiO nanoparticles. In case of NiO nanoparticles, a pre-edge peak at ∼531.5 eV is due to the hybridization of O 2p orbitals with Ni 3d states and higher energy broad spectral features (∼537 eV) are attributed mainly to the O 2p hybridization with Ni 4sp orbitals [38, 39]. For the unimplanted sample of SiO_2, only broad spectral features around ∼537 eV are observed. In the implanted samples up to the dose value 1×10^{16} ions cm^{-2}, the O K-edge NEXAFS spectra are almost similar to the SiO_2 sample. For the higher dose samples, a pre-edge peak at ∼530.7 eV starts to appear and its intensity increases with Ni implantation dose, suggesting a strong hybridization of O 2p orbitals with Ni 3d states. The spectral features of samples having dose values of 1×10^{17} and 2×10^{17} ions cm^{-2} are well matched with the spectrum of NiO nanoparticles. These results are further confirmed by measuring the Ni $L_{3,2}$-edge spectra. Figure 6 shows the normalized spectra of the Ni $L_{3,2}$-edge for all the investigated samples. The intensity of L_3 and L_2 peaks increases with Ni concentration. If the Ni forms some compounds with either oxygen or Si in these materials, under the crystal field splitting effect, the L_3 peak will split into two peaks due to the transition from t_{2g} and e_g 3d orbitals. It is clear from figure 6 that at higher ion dosages (1×10^{17}, 2×10^{17} ions cm^{-2}), a weak shoulder-like feature appears at the L_3-edge, which is closely related to the spectral profiles of NiO reported by Medarde *et al* [39]. The results of the O K- and Ni $L_{3,2}$-edge therefore suggest that at lower implantation doses the probability of forming the NiO phase is less than at higher ion doses, hence validating our HRXRD and optical absorption data. However, we note that the soft energy of the x-rays (at O K- and L-edges) is very sensitive to the surface and the possibility that Ni ions are oxidized cannot be ruled out completely. To avoid surface effects, we used hard x-rays at the K-edge ($1s \rightarrow p$) of Ni ions. Moreover, the details of the Ni atoms interaction to form metallic clusters as well as complexes with O and/or Si in the SiO_2 matrix can also be studied by measuring the Ni K-edge for these samples.

Figure 7 shows the normalized x-ray absorption spectra of the Ni–K edge for the implanted samples along with Ni metal foil and NiO nanopowder as reference compounds. It is well known that different threshold energy inflection

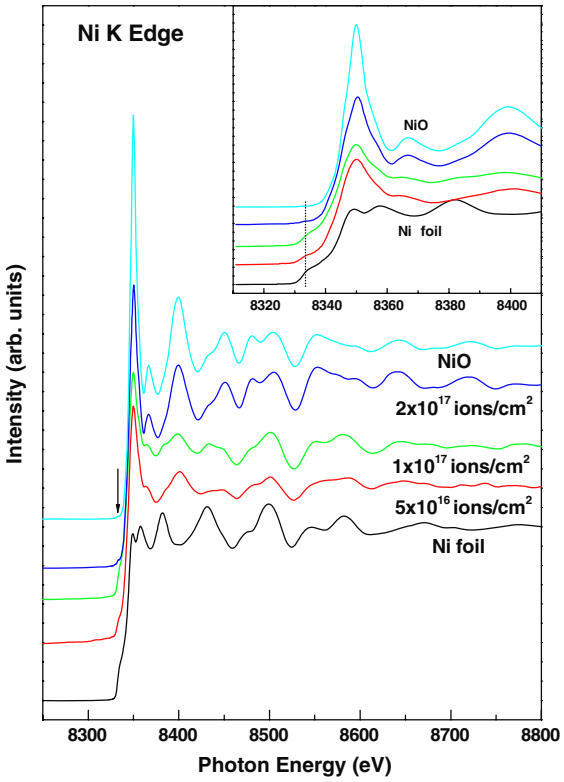

Figure 7. Normalized spectra of Ni K-edge near x-ray absorption fine structure (NEXAFS) spectra of Ni implanted samples at different doses.

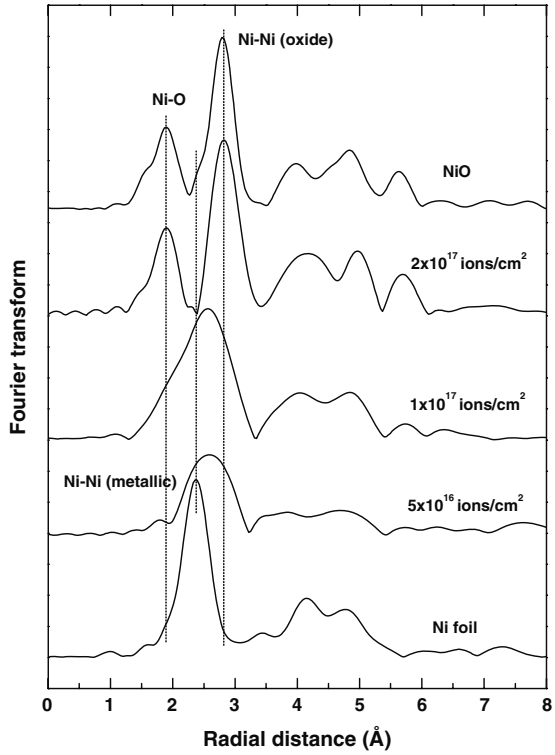

Figure 8. FT amplitudes of k^2-weighted Ni K-edge EXAFS of Ni implanted samples along with Ni metal foil and NiO nanopowder for comparison.

points in the spectra provide the differences in the electronic configurations present in the ground state and on the formal Ni oxidation states. As evident from figure 7, the spectral features of lower ion dose (5×10^{16} ions cm^{-2}), show a very close correspondence to Ni metal foil, whereas the spectra at the highest dose (2×10^{17} ions cm^{-2}) is almost similar to the NiO nanopowder, which point towards the formation of the NiO phase. It is also worth noting that the spectral evolutions of the pre-edge features may occur corresponding to 1s–3d transitions with considerable mixing of 3d–4p states and signify the degree of centrosymmetry of the Ni atom environment. The highest dose sample clearly shows a pre-edge peak (marked by an arrow), as observed in the NiO nanopowder, while the pre-edge features of low ion dose samples are more or less similar to Ni metal foil. These results are in good agreement with the results reported in the literature [40]. The detailed features of NEXAFS regions are shown in the inset of the figure 7. The energy of the main peak does not show any shifts for these samples and is equivalent to the NiO reference spectrum, indicating that Ni is in a divalent state. The main peak and shoulders of the absorption edge correspond to transitions to 4p continuum states and shape resonances of the metal atom environment. For a given environment, the main peak is broadened by disorder in the nearest neighbor distances. The secondary peaks occurring at a few 10 eV above the main peak correspond to multiple scattering from neighboring atom shells. We observed that the spectral profiles of the secondary multiple scattering peaks become less sharp with a decrease in ions dose, thus indicating a significantly less regular Ni environment for the lower dose samples. The structure of Ni atoms can be more clearly visualized by performing a Fourier transform (FT) of the k^2-weighted EXAFS of the Ni-SiO_2 nanocomposite. If there is any interaction between the nanostructure and the matrix, some differences between the spectrum of the nanocomposite and that of the bulk NiO nanopowder, Ni metal foil should emerge. Figure 8 shows the FT amplitudes of k^2-weighted Ni K-edge EXAFS of the implanted samples as well as that of a Ni metal foil and NiO nanopowder for comparison. The FT represents a pseudo-radial distribution function around the Ni atoms, where the r-values are shifted by small amount due to the phase shift of the photoelectron wavefunction. The positions of the FT peaks do not represent the real atomic distances as the FT plotted in figure 8 is not corrected for the backscattering phase shifts in order to present the raw data. As can be seen in figure 8, the first several shells are clearly visible for all the studied samples, suggesting a long range structural order around Ni atoms. The sample of highest dose (2×10^{17} ions cm^{-2}) displays its first peak at around 1.5 Å in FT, corresponding to the Ni–O interaction in the first coordination sphere. The second peak at ~2.5 Å is due to Ni–Ni interactions in the second coordination sphere. The similar peaks at the same distances are shown for NiO nanopowder, which indicate that Ni atoms in this sample have similar local symmetry to that of NiO. The samples having lower ion doses show a significant variation of Ni–Ni interactions, while the Ni–O interactions become negligible as the ion dose decreases. The

contribution of the Ni–O interaction is almost negligible for the dose of 5×10^{16} ions cm^{-2}. Previously, using the same analysis method the structural evolutions of NiO–SiO_2 nanocomposite have done by Corrias *et al* [41], confirming no interaction of NiO nanoparticles with the silica network. However, in the present study, Ni–Ni bond distances change with ion dose and are different from that observed in Ni metal foil. The results therefore suggest that Ni particles are embedded in the empty space of the SiO_2 network with a strong interaction. Hence, one can say that Ni in these samples has a tendency to form a structure to some extent with a coordination similar to that in metal nickel. The different Ni–Ni interaction can be attributed to a varying size of the domain particles of nanometric order. The difference in the amplitude between the samples and the thick Ni foil is probably due basically to the effect of thickness and perhaps a slightly different Debye–Waller factor, which could vary with ion dose. The decreased Ni–Ni interatomic distance with decreasing ion dose increases the overlap of the electron's wavefunctions, leading to a greater charge transfer. It is worth mentioning that, due to the low concentration of Ni ions, the full structure cannot be completed. Therefore, one cannot completely rule out the possibility of Ni atoms doping the Si structure and starting to form nickel silicide compounds.

4. Conclusions

The formation of Ni nanoparticles embedded in a SiO_2 matrix and their growth and saturation to form NiO using ion implantation and annealing was presented. The growth of Ni nanostructures and their oxide formation were characterized by means of various techniques such as HRXRD, UV–visible absorption spectroscopy, dc magnetization, AFM/MFM and x-ray absorption spectroscopy. The detailed investigations of the local structures at various stages of the growth were made using Ni K-edge NEXAFS/EXAFS. These results suggested that the size of the Ni nanoparticles changes with the ion dose, reaching saturation in the form of NiO nanoscopic structure at a dose of 2×10^{17} ions cm^{-2}.

Acknowledgments

The authors are very grateful to Dr A Roy, Director of the Inter University Accelerator Centre, New Delhi for his keen interest and encouragement in this work. SKS and MK are very grateful to FAPESP and CNPq (Brazil) for providing financial support. WKC is grateful for the financial support from KIST under contract 2E19880.

References

[1] Chen W, Ahmed H and Nakazoto K 1995 *Appl. Phys. Lett.* **66** 3383
[2] Meldrum A, Haglund R F Jr, Boatner L A and White C W 2001 *Adv. Mater. (Weinheim, Ger.)* **13** 1431
[3] Lobotka P, Derer J, Vavra I, de Julian Fernandez C, Mattei G and Mazzoldi P 2007 *Phys. Rev.* B **75** 024423
[4] Hache F, Ricard D, Flytzanis C and Kreibig U 1988 *Appl. Phys.* A **47** 347
[5] Fukumi K, Chayahara A, Kodono K, Sakaguchi T, Horino Y, Miya M, Hayakawa J and Satou M 1991 *Japan. J. Appl. Phys.* 2 **30** L 742
[6] Mazzoldi P, Arnold G W, Battaglin G, Gonella F and Hagland R F Jr 1996 *J. Nonlinear Opt. Phys. Mater.* **5** 285
[7] Isobe T, Weeks R A and Zuhr R A 1998 *Solid State Commun.* **105** 469
[8] Morrish A H 1965 *The Physical Principle of Magnetism* (New York: Wiley)
[9] Kechrakos D and Trohidou K N 2005 *Phys. Rev.* B **71** 054416
[10] Denardin J C, Knobel M, Zhang X X and Pakhomov A B 2003 *J. Magn. Magn. Mater.* **262** 15
[11] Chakraborty P 1998 *J. Mater. Sci.* **33** 2235
[12] Comini E 2006 *Anal. Chim. Acta* **568** 28
[13] Bennewitz R 2006 *J. Phys. Condens. Matter* **18** R417–35
[14] Gong W, Li H, Zhao Z and Chen J 1991 *J. Appl. Phys.* **69** 5119
[15] Cintora-Gonzalez O, Estournes C, Muller D, Gullie J L and Grob J J 1999 *Nucl. Instrum. Methods* B **147** 422
[16] Cattaruzza E, Gonella F, Mattei G, Mazzoldi P, Gatteschi D, Sangregorio C, Falconieri M, Salvetti G and Battaglin G 1998 *Appl. Phys. Lett.* **73** 3652
[17] Nakajima A, Futatsugi T, Horiguchi N and Yokoyama N 1997 *Appl. Phys. Lett.* **71** 3654
[18] Magruder R H III, Yang L, Haglund R F Jr, White C W, Yang L, Dorsinville R and Alfano R R 1993 *Appl. Phys. Lett.* **62** 1730
[19] Hole D E, Townsend P D, Barton J D, Nistor L C and van Landuyt J 1995 *J. Non-Cryst. Solids* **180** 266
[20] Liu Z, Li H, Feng X, Ren S, Wang H, Liu Z and Lu B 1998 *J. Appl. Phys.* **84** 1913
[21] Isobe T, Park S Y, Weeks R A and Zuhr R A 1995 *J. Non-Cryst. Solids* **189** 173–80
[22] Maurizio C, Longo A, Martorana A, Cattaruzza E, D'Acapito F, Gonell F, De Julian C, Mattei G, Padovani S and Boesecke P 2003 *J. Appl. Crystallogr.* **36** 732
[23] Amekura H, Umeda N, Takeda Y, Lu J, Kono K and Kishimoto N 2005 *Nucl. Instrum. Methods. Phys. Res.* B **30** 193
[24] Ding X Z, Tay B K, Shi X, Chiah M N F, Cheung W Y, Wong S P, Xu J B and Wilson I H 2000 *J. Appl. Phys.* **88** 2745
[25] Kumar P, Rogrigues G, Lakshmy P S, Kanjilal D, Singh B P and Kumar R 2006 *Nucl. Instrum. Methods* B **252** 354
[26] Kreibig U and Vollmer M 1995 *Optical Properties of Metal Clusters* (*Springer Series in Materials Science* vol 25) (Berlin: Springer)
[27] Bohren C F and Huffman D R 1983 *Absorption and Scattering of Light by Small Particles* (New York: Wiley)
[28] Ravel B and Newville M 2005 *J. Synchrotron Radiat.* **12** 537
[29] Arnold G W and Borders J A 1977 *J. Appl. Phys.* **48** 1488
[30] Malitson I H 1965 *J. Opt. Soc. Am.* **55** 1205
[31] Johnson P B and Christy R W 1974 *Phys. Rev.* B **9** 5056
[32] Creighton J A and Eadon D G 1991 *J. Chem. Soc. Faraday Trans.* **L2** 3881
[33] Ehrenreich H, Philipp H R and Olechna D J 1963 *Phys. Rev.* **131** 2469
[34] Shiga M 1969 *Kotai Butsuri* **4** 641
[35] Fujimori A and Minami F 1984 *Phys. Rev.* B **30** 957
[36] Barzilai S, Goldstein Y, Balberg I and Helman J S 1981 *Phys. Rev.* B **23** 1809
[37] Denardin J C, Brandl A L, Knobel M, Panissod P, Pakhomov A B, Liu H and Zhang X X 2002 *Phys. Rev.* B **65** 064422
[38] Van der Laan G, Zaanen J, Sawatzky G A, Karnatak R and Esteva J M 1986 *Phys. Rev.* B **33** 4253
[39] Medarde M, Fontaine A, Garcia-Munoz J L, Rodriguez-Carvajal J, de Santis M, Sacchi M, Rossi G and Lacorre P 1992 *Phys. Rev.* B **46** 14975
[40] Takenaka S, Umebayashi H, Tanabe E, Matsune H and Kishida M 2007 *J. Catal.* **245** 392
[41] Corrias A, Mountjoy G, Piccaluga G and Solinas S 1999 *J. Phys. Chem.* B **103** 10081